Publishing Excellence Inspiring Progress
ARISTON PUBLICATIONS
MatSci Express
ISSN: 2997-8440 www.aristonpubs.com/matsci-express https://doi.org/10.69626/mse.2024.0151

RESEARCH ARTICLE

First Principle Study of Tunnel Magnetoresistance of Various Oxide Materials

Sharif Saleem, Gul Faroz Ahmad Malik, Amir Farooq, Farooq Ahmad Khanday*

ABSTRACT: In this paper, the first principle study of tunnel magnetoresistance (TMR) for various oxide materials has been done. More than 30 materials have been taken into consideration and divided into four different categories based on their bandgap. The four categories are 2-4 eV bandgap materials, 4-6 eV bandgap materials, 6-8 eV bandgap materials, and 8-10 eV bandgap materials. The first principle simulations and the device-level simulations of various MTJ configurations were executed using the various oxide materials. The results reveal that maximum TMR ratio is observed in oxide materials having lower bandgap value and it reduces with the increase in oxide material bandgap. The maximum TMR ratio is observed in Cu_2O material and minimum TMR is observed in BeO material. The oxide materials with bandgap less than 3 eV are the best materials for device level fabrication and they provide 100% TMR for the oxide thickness up to 3 nm.

Keywords: Spintronics, Magnetoresistance, TMR, Magnetic Tunnel Junction.

Received: 23 March 2024; Revised: 27 April 2024; Accepted: 06 May 2024; Published Online: 11 July 2024

1. INTRODUCTION

Metal oxide semiconductor field effect transistor (MOSFET) is the building block of modern electronics and is frequently manufactured device [1]. The scaling and miniaturization of MOSFET increases the growth of the semiconductor technology drastically and enables high-density integrated circuits (ICs) like memory chips and microprocessors [2]. MOSFET is a priary element of memory and the emergence of this device enables the use of metal oxide semiconductor (MOS) transistor as memory cell. John Schmidt developed the first MOS based memory in 1965. It was 64-bit metal oxide semiconductor static random access memory (MOS SRAM) [3]. This memory requires six transistors for each data bit. Later it was found that MOSFETs have ability to build capacitors that can store charge [4]. This property enables to write the charge either 1 or 0 and the MOS transistor could control writing the charge to capacitor. This leads the way to the development of dynamic random access memory (DRAM) cell. The prime advantages of MOS memory were high efficiency, cost effective, and less power requirement. These memories are widely used in analog storage, basic input/output system (BIOS) storage, cache memory, floating gate memory, and so on [5-9].

With the advancement in technology and when the technology node shrinks beyond 45 nm, power dissipation and performance becomes important concerns [1]. As the size of chips get reduced, the size of MOS capacitor also reduces. By scaling MOSFET, several limitations arise, such as subthreshold leakage current, time dependent dielectric breakdown, hot electron effects and several other short channel effects. Apart from these limitations, the main problems with the MOS technology are power dissipation and volatility.

There are several other technologies and alternate devices to reduce the power at circuit level. Some alternate devices are double gate MOSFET (DG-MOSFET), fin field-effect transistor (FIN FET), tunnel field-effect transistor (TFET), spin field-effect transistor (SPIN FET) and carbon nanotube field-effect transistor (CNT-FET) [2-5]. The alternate technologies are as straintronics, spintronics etc. [6-7]. By all these methods several logics were developed [8], but all those logics suffer volatility problem.

To overcome these problems industries look for some better replacement. Spintronics is the technology, which has

Department of Electronics and Instrumentation Technology, University of Kashmir, Hazratbal, Srinagar-190006, Jammu and Kashmir, India.

* Author to whom correspondence should be addressed: farooqkhanday@kaghmiruniversity.ac.in (F. A. Khanday)

capability to overcome both the issues of power dissipation and volatility. It is an emerging technology and have ability to enhance the future of electronics [9]. Apart from mass and charge, electrons have another basic property, i.e., spin. Spin is a pseudo vector quantity that has a predetermined magnitude of $\frac{\hbar}{2}$ and has a variable polarization. ħ is reduced Plank's constant. However in past spin and charge have been treated separately. In classical electronics, information is stored in capacitors in the form of charge to save it and the charge of an electron is moved by electric field. In other standard technologies such as magnetic recording electron spin is used only through their macroscopic illustration. This technology exploits the spin property of an electron to encode information [10].

In charge based devices to switch from logic 0 to 1, the magnitude of charge is changed so current can flow from drain to source that makes it impossible to reduce the power dissipation as charge is a scaler quantity. On the other hand, in spintronic switching is attained by inverting the spin polarization without any change in the flow of current [11]. Some commonly used spintronic devices are spin field-effect transistor (spin FET), spin valve, spin MOSFET, spin tunnel field-effect transistor (spin TFET), magnetic tunnel junction (MTJ), spin transfer torque random access memory (STT-RAM), and so on [12-16].

Magnetic tunnel junction (MTJ) is a spin based device which provides some important features like non- volatility, low power consumption and increased integration densities [17-30]. In past few years, researchers have shown the future of MTJs in many areas. Due to its non-volatility property, it is used as memory devices like Magnetic random access memories (MRAM) and Static Random Access Memories (SRAM) [18].

Scientists discovered an MTJ, Fe/Ge/Co, which provides the TMR ratio of about 14% at low temperature [19]. Ni/Nio/(Ni, Fe, Co) based MTJ was also reported in the literature, which demonstrated very low TMR at room-temperature [20]. A MTJ with the TMR ratios >10% at room-temperature was obtained in amorphous Al-oxide barrier and reported in the literature [21, 22] With the passage of time, TMR goes on increasing consistently year after year and reached up to 70% which is maximum TMR obtained using AlO barrier. After AlO barriers, the researchers move towards MgO barriers. The MgO barrier MTJ's provides TMR ratio >90% [23, 24]. In order to achieve high TMR ratio in MgO-based MTJ's, it requires epitaxial growth of the MgO layer and correct crystalline orientation on ferromagnetic electrodes, which is very difficult. There are several other MTJ's with different barrier materials like $Fe/MgAl_2O_4/Fe$ [25]. Table 1 provides a comparative study of different MTJ devices reported in the literature with regards to magnetoresistance ratio.

The Fe/MgO/Fe MTJ configuration can provides 100% TMR ratio [25] but only at few atomic levels. This configuration provides 100% TMR ratio for oxide thickness 1nm to 1.2 nm. In this paper, it has been observed that materials with lower bandgap value provides 100% TMR ratio for oxide thickness 1nm to 2 nm. E.g., Cu_2O etc.

The electrical control of magnetization in MTJs present significant progresses like speed, reliability, non-volatility, high efficiency of control and scalability. Tunnel Magnetoresistance TMR is an important parameter of MTJ. It is the electrical resistance of MTJ that depends on the layers and magnetic alignment of device [26-28]. For good quality readability and fast switching high TMR value is required. From the first experimental demonstration of TMR effect, [29] it was found that TMR value of MTJ also depends on the tunnel barrier quality.

Table 1. Comparative study of different MTJ devices reported in the literature with regard to magnetoresistance ratio.

MTJ Configurations	Tunnel magneto-resistance ratio	Ref.
$Co/Al_2O_3/Alq_3/Co$	19%	[26]
Fe/MgO/Fe	100%	[25]
$Fe/Y_2O_3/Fe$	85%	[25]
$Fe/Al_2O_3/Fe$	90%	[25]
$Fe/HfO_2/Fe$	<100%	[25]
CoFeB/Al-O/CoFeB	80%	[27]
CoFeB/MgO/CoFeB	49.7%	[28]
Fe/MgO/FeCo(001)	60%	[29]
FeCo/MgO/FeCo	80%	[30]
This work	100%	

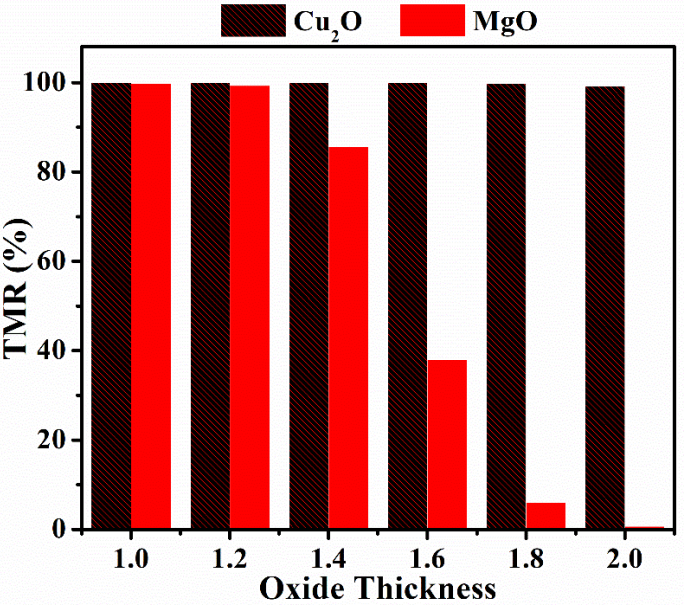

Fig. 1. Bar graph of Cu_2O and MgO.

With the emergence of big data and the unconventional computing, technologies require less time for writing data, storing them at a smaller scale with less energy consumption. This becomes the main driving force for MTJ research.

In this paper more than 30 materials have been analyzed and we found a strong relation between the bandgap of oxide

material used and TMR of the MTJ. The materials were categorized on the basis of their bandgap and have been divided into four categories, 2-4 eV bandgap materials, 4-6 eV bandgap materials, 6-8 eV bandgap materials, and 8-10 eV bandgap materials. We perform the device-level simulations of these oxide materials using tool nanoHUB and obtain various results.

The results reveal that maximum TMR ratio is observed in oxide materials having lower bandgap value and it reduces with the increase in oxide material bandgap. It has been observed that oxide materials with lower bandgap value like Cu_2O, Tl_2O_3, CdO, HgO, PbO, Bi_2O_3, NiO are the best materials for device level fabrication and they provide 100% TMR for the oxide thickness up to 3nm.

2. MODELS AND METHODS

MTJ is an important spintronic device used for various logic and memory applications. Its working principle combines the magnetism and electronics and provides high speed, non-volatility and infinite tolerance. The basic principle of MTJ is tunneling magneto-resistance. In comparison with other non-volatile memories like NAND, Re-RAM and Pc-RAM , MTJ requires small write voltage 0.3V-0.4V, less write time 0.5-10 ns, less read time <5 ns and endurance up to 10^{15}.

MTJ is a three-layer device. It contains an insulator layer, which is sandwiched between two ferromagnetic materials. The insulator layer thickness is up to 2 nm and is made of materials like AlO, MgO, SiO_2, ZnO, CdO, and high k materials etc. [31, 32]. The ferromagnetic layers thickness is up to 10nm and materials used for these layers are iron, nickel, cobalt, boron and Heusler alloys, and so on [33]. The lower ferromagnetic layer contains the electronics that have the same spin and is called as fixed layer or reference layer. The upper ferromagnetic layer contains electrons that change their spin in response to an external magnetic field or through a phenomenon called as spin transfer torque (STT). This layer is called as free layer. When the spin of ferromagnetic layers is parallel the structure stores a 1 and when spin of ferromagnetic layers is opposite the structure stores a 0 [34, 35].

To read the data whether its 0 or 1, a small current is applied to MTJ structure. If the spins of the fixed layer and free layer are, parallel electrons can pass through the barrier, the resistance offered by the device for the flow of read current is less and it is denoted by parallel resistance R_P. When the spins are antiparallel, almost no electronics can tunnel through the barrier, the device offers more resistance to the flow of read current, and is denoted by antiparallel resistance R_{AP}. The resistance variation of the two states R_P and R_{AP} of the device is represented by the tunnel magnetoresistance (TMR).

$$TMR = \frac{R_{AP} - R_P}{R_P}$$

Depending upon the material, different MTJ's, exhibit different Spin-polarization and hence different spin dependent tunneling. In order to calculate the percentage change in junction resistance we measure TMR ratio by below given equation [36-40].

$$TMR \quad ratio = \frac{R_{AP} - R_P}{R_{AP}} \times 100$$

By the recommendation of CA-PZ, Local density Approximation (LDA) has been used to evaluate the exchange-correlation energy [21]. The wave function is prolonged for plane-wave cutoff energy of about 300 eV for doped and undoped samples. In both of the samples, 5×5×6 k-points has been applied to maintain the standards of convergence in calculating electronic characteristics and geometry optimization. Vanderbilt type ultrasoft pseudopotential has been described the electron-ion interaction. BFGS (Broyden-Fletcher-Goldfarb-Shanno) relaxation plan has been employed to optimize the dwelling.

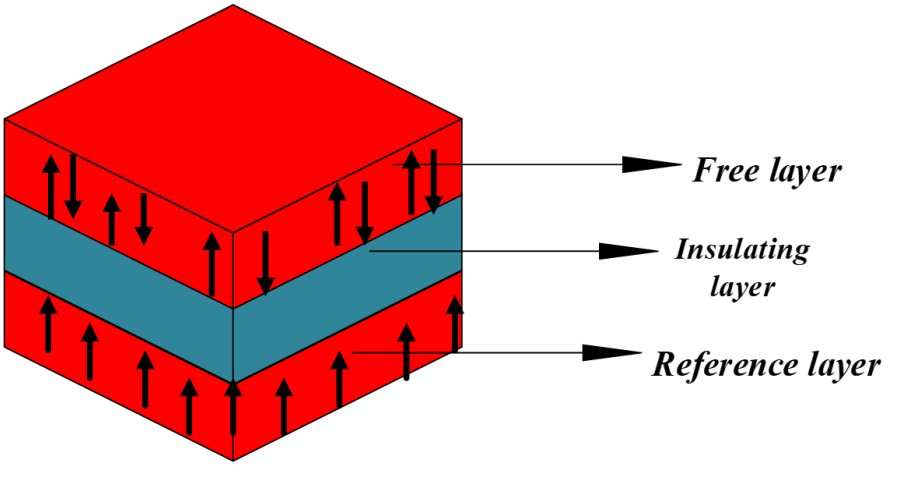

Fig. 2. Basic structure of MTJ.

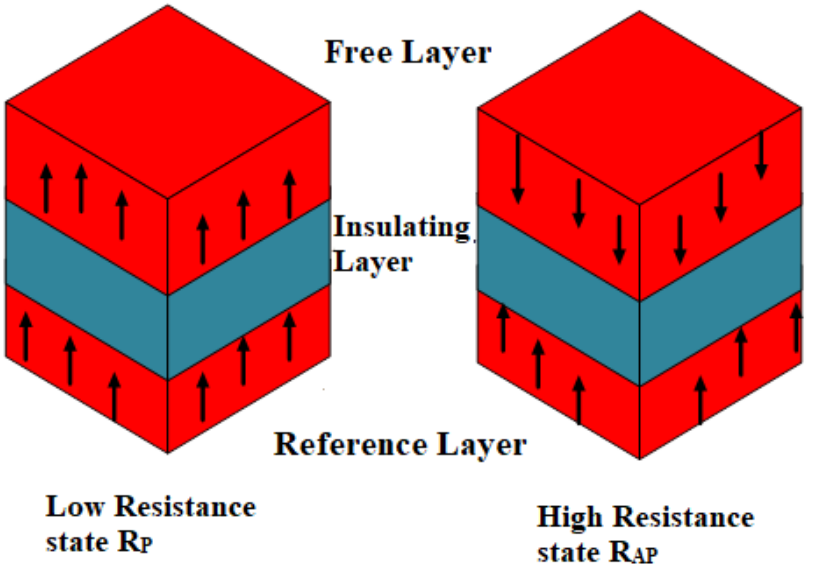

Fig. 3. Front view of MTJ switching from low resistance state to high resistance state.

The calculations are carried out on a unit cell and supercell. In addition, the molecular optimizations have been determined since the residual forces are below 0.05 eV. Geometry is optimized when total energy is 2×10^{-5} eV/atom, the pressure is the most (0.05 eV/Å), maximum stress is 0.1 GPa as well as the maximum atomic displacement is roughly 1.0×10^{-3} Å. All the calculations are actually run parallel to three occasions.

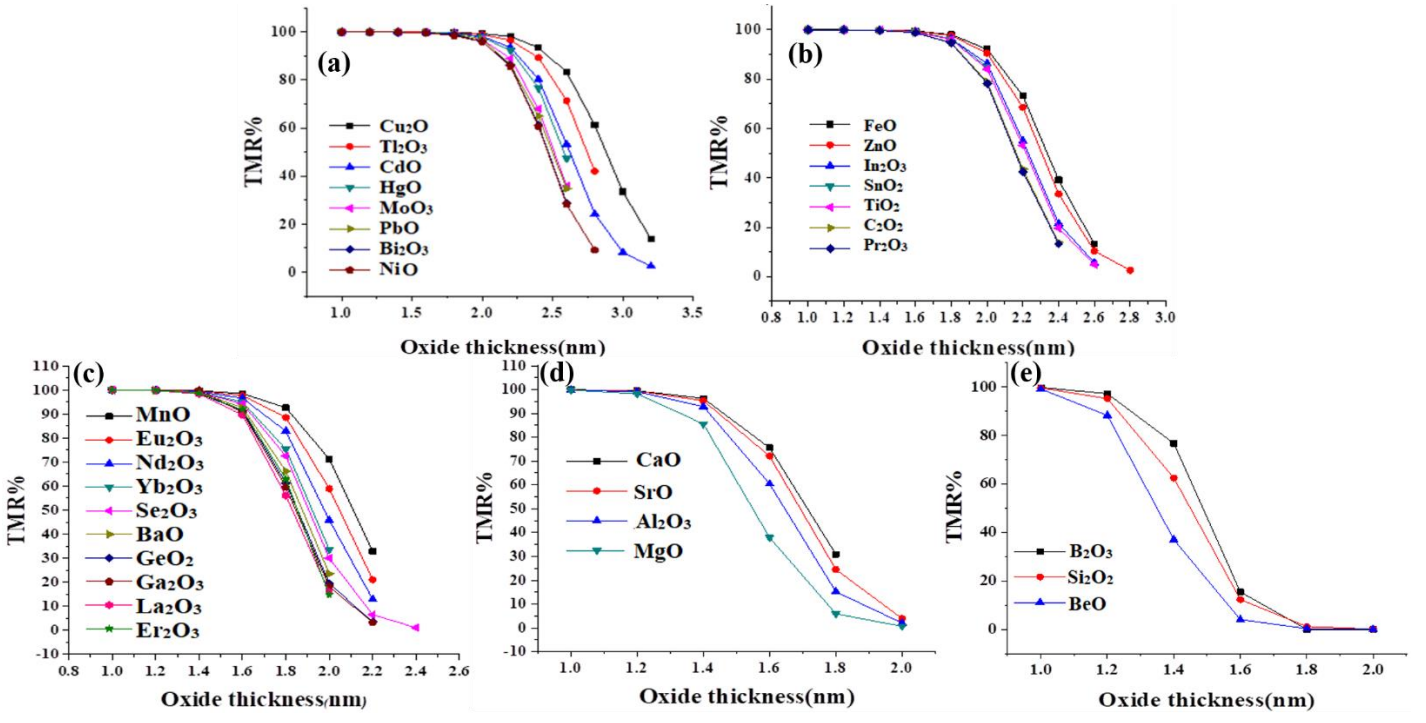

Fig. 4. (a) TMR vs oxide thickness of MTJ configurations having bandgap 2-3 eV. (b) TMR vs oxide thickness of MTJ configurations having bandgap 3-4 eV. (c) TMR vs oxide thickness of MTJ configurations having bandgap 4-6 eV. (d) TMR vs oxide thickness of MTJ configurations having bandgap 6-8 eV. (e) TMR vs oxide thickness of MTJ configurations having bandgap 8-11 eV.

3. RESULTS AND DISCUSSION

Fig. 4 (a-e) exhibit the TMR ratio Vs oxide thickness plots of the various MTJ configurations in parallel and anti-parallel magnetized states respectively. From these plots, it is clearly shown that with small bandgap oxide materials, the TMR ratio is very high up to 100%. These results clearly reveal that the oxide material with least bandgap value, below 5 nm provides the highest TMR ratio up to 100% and provide constant results for large oxide thickness up to 3 nm.

Fig. 5 shows the TMR plot of materials having bandgap 2-3 eV. It is clearly seen that these materials provide the TMR ratio up to 100% and provide constant results for oxide thickness up to 3 nm. The bandgap of Cu_2O oxide material is 2.04 that is least among all materials. This material provides best results among all materials as shown in figure 3.2 and can be used for device level fabrication. It is seen from the plot that Fe/Cu_2O/Fe MTJ exhibits 100% TMR ratio constantly even when the insulator thickness is increased from 1nm to 2.6nm. The other MTJ configurations having oxide materials like Tl_2O_3, CdO, HgO, PbO, Bi_2O_3, NiO also exhibits similar characteristics.

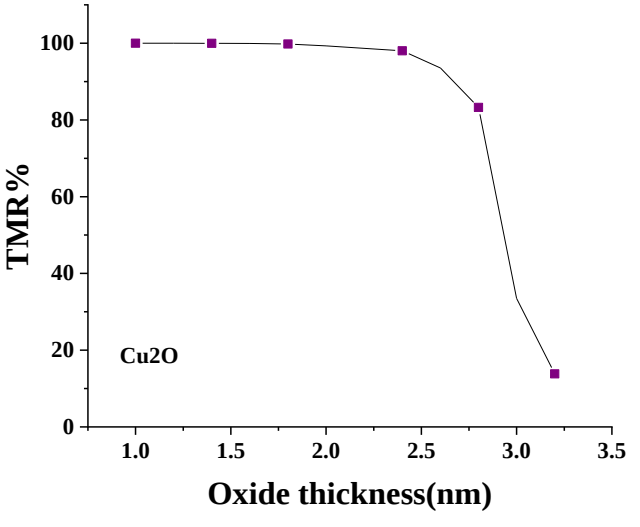

Fig. 5. TMR ratio vs oxide thickness of Cu_2O.

The second category of the materials that have been considered in this paper are the materials having bandgap 3-4 eV. The results of this category are also similar to the above materials but provides 100% TMR ratio for the insulator thickness less than 2 nm only. This category includes oxide materials like FeO, ZnO, In_2O_3, SnO_2, TiO_2, Pr_2O_3 etc.

Fig. 6 shows TMR ratio vs oxide thickness of FeO. This material shows 100% TMR ratio for oxide thickness 1 nm - 2 nm. This material provides the best results in this category and can be used for device level fabrication of MTJ. The other categories of materials that are taken in this paper are the materials having bandgap 4-6 eV, materials having bandgap 6-8 eV and materials having bandgap 8-11 eV. These materials provide the similar characteristics as of first two categories but the only difference is that highest TMR is obtained only for few atomic levels of the oxide. The 100% TMR ratio is obtained only for oxide thickness of 1-1.4 nm.

The materials having bandgap above 6 eV, results are not same. In these materials, the highest TMR ratio obtained is 90% and can be obtained at one or two atomic levels of oxide material.

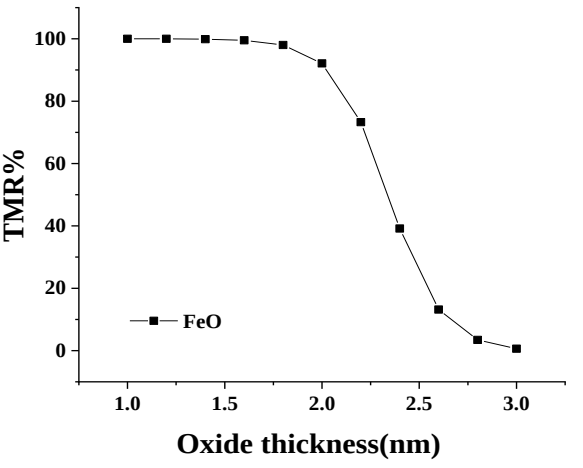

Fig. 6. TMR ratio vs oxide thickness of FeO.

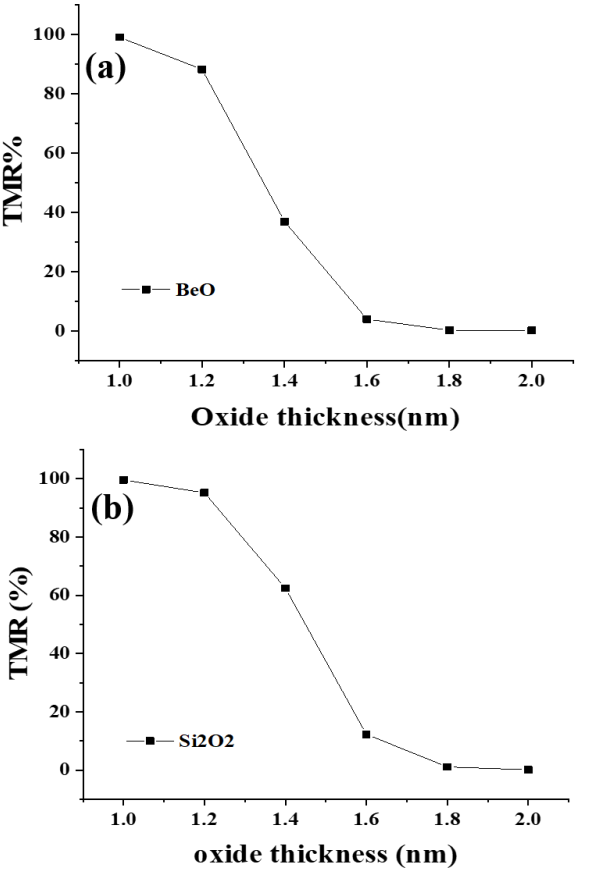

Fig. 7. TMR ratio vs oxide thickness of BeO and Si_2O_2.

Fig. 7 (a) and (b) shows the plot of TMR ratio vs oxide thickness of BeO and Si_2O_2. Both the materials provide highest TMR 100% only at 1nm and then decreases with the increase in the oxide thickness. At 1.8 nm, the TMR ratio is almost zero. From the above plot it is clearly seen that these materials are not best for MTJ device fabrication, because these materials provide 100% TMR only at 1nm oxide thickness.

Table 2. R_P and R_{AP} TMR ratio of various MTJ configurations.

Material	Parameters	Oxide thickness					
		1	1.2	1.4	1.6	1.8	2
Cu_2O	Parallel resistance R_P (Ω)	679.8	2148.8	6798.6	21492.4	67810.3	213063
	Anti-parallel resistance R_{AP}(Ω)	33661000	33917700	33825100	33705100	33593600	31053100
	TMR%	99.99	99.99	99.97	99.93	99.79	99.31
Tl_2O_3	Parallel resistance R_P (Ω)	940.9	3158	10606.9	35580	119049	399684
	Anti-parallel resistance R_{AP}(Ω)	37962200	38006200	37903200	37778100	37664700	37568600
	TMR%	99.99	99.98	99.97	99.90	99.68	98.93
CdO	Parallel resistance R_P (Ω)	1362.6	4894	17576	63027	225185	795948
	Anti-parallel resistance R_{AP}(Ω)	43456400	43201600	43005100	42851400	42729400	42631100
	TMR%	99.99	99.98	99.95	99.85	99.47	98.13
HgO	Parallel resistance R_P (Ω)	1528.6	5606.9	20553.7	75236.7	274253	9870011
	Anti-parallel resistance R_{AP}(Ω)	44742400	44761800	44643000	44511000	44395200	44298600
	TMR%	99.99	99.98	99.95	99.83	99.38	97.77
MoO_3	Parallel resistance R_P (Ω)	4914	7312	27916	106366	403055	1499850
	Anti-parallel resistance R_{AP}(Ω)	48521500	48273700	48078400	47924800	44334700	47704800
	TMR%	99.99	99.98	99.94	99.77	99.09	96.85
PbO	Parallel resistance R_P (Ω)	1941.2	7433.1	28447.3	108656	412709	1538800
	Anti-parallel resistance R_{AP}(Ω)	48389900	48395300	48268900	48133900	48017100	47920300
	TMR%	99.99	99.98	99.94	99.77	99.14	96.78
Bi_2O_3	Parallel resistance R_P (Ω)	2227.2	8741.1	34284.8	134175	521628	1981770
	Anti-parallel resistance R_{AP}(Ω)	50583300	50580300	50449700	50195700	5009800	50618700
	TMR%	99.99	99.98	99.93	99.73	98.96	96.044
NiO	Parallel resistance R_P (Ω)	2257	8882	34924	137008	533859	2031860
	Anti-parallel resistance R_{AP}(Ω)	51132900	50887500	50692400	50538800	50417000	50318400
	TMR%	99.99	99.98	99.93	99.72	98.44	95.96
FeO	Parallel resistance R_P (Ω)	3541	15100	64320	273028	1144700	457500
	Anti-parallel	58809100	58567700	58372300	58218300	58096500	57998500

	resistance $R_{AP}(\Omega)$						
	TMR%	99.99	99.99	99.88	99. 53	98.02	92.11
ZnO	**Parallel resistance R_P (Ω)**	45074.3	196639	856798	3718450	15900900	64135700
	Anti-parallel resistance $R_{AP}(\Omega)$	681868000	681404000	679748000	678149000	676814000	675724000
	TMR%	99.99	99.97	99.87	99.45	97. 66	90.50
In_2O_3	**Parallel resistance R_P (Ω)**	5496.9	25347.8	116698	534256	2390280	9732960
	Anti-parallel resistance $R_{AP}(\Omega)$	66896100	66834000	66677900	66532400	66412400	66314900
	TMR%	99.99	99.96	99.82	99.16	96.40	85.32
SnO_2	**Parallel resistance R_P (Ω)**	5633	26088	120629	554546	2489360	10134500
	Anti-parallel resistance $R_{AP}(\Omega)$	67614800	67373900	67177200	67022600	69900600	66802600
	TMR%	99.99	99.96	99.82	99.17	96.43	84.82
TiO_2	**Parallel resistance R_P (Ω)**	5842	27236	126751	734698	2644930	10761900
	Anti-parallel resistance $R_{AP}(\Omega)$	68348900	68108000	67911100	67572950	67634400	67456300
	TMR%	99.99	99.96	99.81	99.02	96.08	84.06
CeO_2	**Parallel resistance R_P (Ω)**	7251	35137	169858	814738	3776830	15198000
	Anti-parallel resistance $R_{AP}(\Omega)$	72815900	72574200	72376500	72221400	72099300	72001300
	TMR%	99.99	99.95	99.77	98.87	94.77	78.89
Pr_2O_3	**Parallel resistance R_P (Ω)**	7428	36123	175395	844618	3926180	15765900
	Anti-parallel resistance $R_{AP}(\Omega)$	73318800	73077000	72879100	72724100	72601900	72503900
	TMR%	99.98	99.95	99.75	98.83	94. 59	78.24
MnO	**Parallel resistance R_P (Ω)**	9384	47578	240609	1203900	5734480	22318600
	Anti-parallel resistance $R_{AP}(\Omega)$	78419000	7817500	77976800	77821300	77699000	77600900
	TMR%	99.98	99.93	99.96	98.44	92. 61	71.23
Eu_2O_3	**Parallel resistance R_P (Ω)**	13182	70975	380809	2010230	9803430	3086800
	Anti-parallel resistance $R_{AP}(\Omega)$	96308800	86062600	85862100	85706000	85583400	85485300
	TMR%	99.98	99.91	99. 55	97. 65	88. 54	58.95
Nd_2O_3	**Parallel resistance R_P (Ω)**	43716	104394	592732	3283590	16073100	50697900
	Anti-parallel resistance $R_{AP}(\Omega)$	94351000	94230900	94028700	93872000	93749200	93650900

	TMR%	99.95	99.88	99.36	96.50	82.84	45.87
Yb_2O_3	**Parallel resistance R_P (Ω)**	25123.2	151587	908516	5248110	25153800	67722000
	Anti-parallel resistance R_{AP}(Ω)	102811000	102655000	102468000	102313000	102191000	102092000
	TMR%	99.97	99.85	99.11	94.87	75.38	33. 66
Se_2O_3	**Parallel resistance R_P (Ω)**	27860. 6	171198	1044130	6106110	28879300	73444000
	Anti-parallel resistanceR_{AP} (Ω)	105693000	105531000	105343000	105188000	105065000	104967000
	TMR%	99.97	99.83	99.00	94.19	72. 51	30.03
BaO	**Parallel resistance R_P (Ω)**	34153	217532	1372730	8203970	37401400	84689500
	Anti-parallel resistance R_{AP}(Ω)	111648000	111390000	111185000	111027000	110903000	110805000
	TMR%	99.96	99.80	98.90	92. 61	66.22	23.56
GeO_2	**Parallel resistance R_P (Ω)**	39683. 5	259526	1678760	10169200	44693700	92835700
	Anti-parallel resistance R_{AP}(Ω)	116013000	115833000	115639000	115483000	115360000	115261000
	TMR%	99.97	99.77	98. 54	91.19	61. 25	19.44
Ga_2O_3	**Parallel resistance R_P (Ω)**	41698	275091	1793930	10909300	47283700	95484000
	Anti-parallel resistanceR_{AP}(Ω)	117516000	117334000	117114000	116983000	116860000	116761000
	TMR%	99.96	99.77	99.89	90. 67	59. 53	18.22
La_2O_3	**Parallel resistance R_P (Ω)**	46007.6	308813	2046270	12529700	52681600	100673000
	Anti-parallel resistance R_{AP}(Ω)	120545000	120385000	120163000	120006000	119882000	119784000
	TMR%	99.96	99.74	98.29	89. 56	56.05	15.94
Er_2O_3	**Parallel resistance R_P (Ω)**	37756.7	244771	1570420	9472920	42181400	90152800
	Anti-parallel resistance R_{AP}(Ω)	114517000	114339000	114146000	113990000	113867000	105614000
	TMR%	99.96	99.78	98.62	91. 68	62.94	14. 63
CaO	**Parallel resistance R_P (Ω)**	94367.9	718343	5313600	32598400	9938100	135753000
	Anti-parallel resistance R_{AP}(Ω)	144499000	144280000	144077000	133605000	143794000	143694000
	TMR%	99.93	99. 502	96.31	75.6	30.88	5.52
SrO	**Parallel resistance R_P (Ω)**	117252	926877	7063990	42399100	114495000	145627000
	Anti-parallel resistance R_{AP}(Ω)	152400000	152174000	15196000	151809000	151685000	151585000
	TMR%	99.92	99.39	95.35	72.07	24.51	3.93

Al_2O_3	**Parallel resistance R_P (Ω)**	175703	1489310	11919700	66213800	141837000	163723000
	Anti-parallel resistance R_{AP}(Ω)	169789000	167749000	167540000	167380000	167255000	167155000
	TMR%	99.89	99.11	92.88	60.44	15.17	2.04
MgO	**Parallel resistance R_P (Ω)**	354897	3386440	28552200	122518000	185484000	195796000
	Anti-parallel resistance R_{AP}(Ω)	197963000	197675000	197459000	197296000	197170000	197069000
	TMR%	99.82	98.28	85.54	37.9	5.92	0.64
B_2O_3	**Parallel resistance R_P (Ω)**	598642	6164980	51703600	164252000	207952000	213209000
	Anti-parallel resistance R_{AP}(Ω)	222406000	222112000	221894000	194217000	218350000	213580000
	TMR%	99.73	97.22	76.69	15.42	4.77	0.17
Si_2O_3	**Parallel resistance R_P (Ω)**	1082280	12255700	95180300	221846000	249820000	252418000
	Anti-parallel resistance R_{AP}(Ω)	253568000	253283000	253065000	252900000	252772000	252670000
	TMR%	99.57	95.16	62.38	12.27	11.67	0.09
BeO	**Parallel resistance R_P (Ω)**	2657600	33328600	192872000	293526000	304823000	305572000
	Antiparallel resistanceR_{AP}(Ω)	306569000	306261000	306038000	305871000	305742000	305639000
	TMR%	99.13	88.24	36.97	4.03	0.3	0.02

4. CONCLUSION

In this paper, we investigated the TMR ratio of various MTJ configurations based on NEGF equations. The first principle study of TMR for various MTJ configurations has been carried out in this paper. We develop the quantum model of MTJ using the NEGF equations. By these simulations, we obtain the TMR verses thickness curves of each MTJ. In this paper, we calculate the TMR ratio of each MTJ and plot it against the thickness of oxide material used. By varying the thickness of oxide material, we observe the changes in TMR ratio. We compare the TMR curves of each MTJ model and obtain the best oxide material that provides the 100% TMR ratio. By these simulations, we also observe that the TMR ratio of an MTJ depends on the bandgap of the insulator material. We observe that the oxide material with the lower bandgap value provides best TMR ratio than the material with the higher bandgap value. We conclude that the oxide materials with lower bandgap value Tl_2O_3, CdO, HgO, PbO, Bi_2O_3, NiO, FeO, ZnO, In_2O_3, SnO_2, TiO_2, Pr_2O_3 provides the TMR ratio up to 100 for thickness of oxide material from 1nm to 3nm. Also the oxide materials with the higher bandgap value La_2O_3, Er_2O_3, CaO, SrO, Al_2O_3, MgO, B_2O_3, Si_2O_3, BeO provides the 100% TMR ratio but for few atomic levels of oxide material, 1nm to 1.4 nm only.

CONFLICT OF INTEREST

The authors declare that there is no conflict of interests.

REFERENCES

[1] Maghroori, M. and Dolatshahi, M., 2021. Design of low-power CMOS VLSI circuits using multi-objective optimization in genetic algorithms. *World Journal of Advanced Research and Reviews*, *12*(1), pp.215-224.

[2] Iwai, H., 2009. Roadmap for 22 nm and beyond. *Microelectronic Engineering*, *86*(7-9), pp.1520-1528.

[3] Dasgupta, A., Agarwal, A. and Chauhan, Y.S., 2017. Unified compact model for nanowire transistors including quantum effects and quasi-ballistic transport. *IEEE Transactions on Electron Devices*, *64*(4), pp.1837-1845.

[4] Goharrizi, A.Y., Pourfath, M., Fathipour, M. and Kosina, H., 2012. Device performance of graphene nanoribbon field-effect transistors in the presence of line-edge roughness. *IEEE Transactions on electron devices*, *59*(12), pp.3527-3532.

[5] Rezali, F.A.M., Othman, N.A.F., Mazhar, M., Hatta, S.W.M. and Soin, N., 2016. Performance and device design based on geometry and process considerations for 14/16-nm strained FinFETs. *IEEE Transactions on Electron Devices*, *63*(3), pp.974-981.

[6] Flatte, M.E., 2007. Spintronics. *IEEE transactions on electron devices*, *54*(5), pp.907-920.

[7] Malik, G.F.A., Kharadi, M.A., Parveen, N. and Khanday, F.A., 2020. Modelling for triple gate spin-FET and design of triple gate spin-FET-based binary adder. *IET Circuits, Devices & Systems*, *14*(4), pp.464-470.

[8] Moaiyeri, M.H., Nasiri, M. and Khastoo, N., 2016. An efficient ternary serial adder based on carbon nanotube FETs. *Engineering Science and Technology, an International Journal*, *19*(1), pp.271-278.

[9] Datta, S. and Das, B., 1990. Electronic analog of the electro-optic modulator. *Applied Physics Letters*, *56*(7), pp.665-667.

[10] Maciel, N., Marques, E., Naviner, L., Zhou, Y. and Cai, H., 2019. Magnetic tunnel junction applications. *Sensors*, *20*(1), p.121.

[11] Joshi, V.K., Barla, P., Bhat, S. and Kaushik, B.K., 2020. From MTJ device to hybrid CMOS/MTJ circuits: A review. *IEEE Access*, *8*, pp.194105-194146.

[12] Kharadi, M.A., Malik, G.F.A., Khanday, F.A. and Shah, K.A., 2020. Hydrogenated silicene based magnetic junction with improved tunneling magnetoresistance and spin-filtering efficiency. *Physics Letters A*, *384*(32), p.126826.

[13] Tahara, T., Koike, H., Kameno, M., Sasaki, T., Ando, Y., Tanaka, K., Miwa, S., Suzuki, Y. and Shiraishi, M., 2015. Room-temperature operation of Si spin MOSFET with high on/off spin signal ratio. *Applied Physics Express*, *8*(11), p.113004.

[14] Dién y, B., 1994. Giant magnetoresistance in spin-valve multilayers. *Journal of Magnetism and Magnetic Materials*, *136*(3), pp.335-359.

[15] Wang, G., Wang, Z., Klein, J.O. and Zhao, W., 2017. Modeling for spin-FET and design of spin-FET-based logic gates. *IEEE Transactions on Magnetics*, *53*(11), pp.1-6.

[16] Turkane, S.M. and Kureshi, A.K., 2016. Review of tunnel field effect transistor (TFET). *International Journal of Applied Engineering Research*, *11*(7), pp.4922-4929.

[17] Sharma, B., Kundu, C., Rahaman, H. and Sarkar, C.K., 2018. Study of TMR with Different Ferromagnetic Material and Variations in Spin-Split, Thickness and Oxide Barrier Height of a MTJ Memory Device. *Journal of Nanoelectronics and Optoelectronics*, *13*(2), pp.245-250.

[18] Parkin, S.S., Kaiser, C., Panchula, A., Rice, P.M., Hughes, B., Samant, M. and Yang, S.H., 2004. Giant tunnelling magnetoresistance at room temperature with MgO (100) tunnel barriers. *Nature materials*, *3*(12), pp.862-867.

[19] Maekawa, S. and Gafvert, U., 1982. Electron tunneling between ferromagnetic films. *IEEE Transactions on Magnetics*, *18*(2), pp.707-708.

[20] Moodera, J.S., Nassar, J. and Mathon, G., 1999. Spin-tunneling in ferromagnetic junctions. *Annual Review of Materials Science*, *29*(1), pp.381-432.

[21] Miyazaki, T. and Tezuka, N., 1995. Spin polarized tunneling in ferromagnet/insulator/ferromagnet junctions. *Journal of Magnetism and Magnetic Materials*, *151*(3), pp.403-410.

[22] Butler, W.H., Zhang, X.G., Schulthess, T.C. and MacLaren, J.M., 2001. Spin-dependent tunneling conductance of Fe| MgO| Fe sandwiches. *Physical Review B*, *63*(5), p.054416.

[23] Mathon, J. and Umerski, A., 2001. Theory of tunneling magnetoresistance of an epitaxial Fe/MgO/Fe (001) junction. *Physical Review B*, *63*(22), p.220403.

[24] Miura, Y., Muramoto, S., Abe, K. and Shirai, M., 2012. First-principles study of tunneling magnetoresistance in $Fe/MgAl_2O_4/Fe(001)$ magnetic tunnel junctions. *Physical Review B*, *86*(2), p.024426.

[25] Dey, D., De, D., Ahmadian, A., Ghaemi, F. and Senu, N., 2021. Electrically doped nanoscale devices using first-principle approach: a comprehensive survey. *Nanoscale research letters*, *16*, pp.1-16.

[26] Gani, M., Shah, K.A., Parah, S.A. and Misra, P., 2020. Room temperature high giant magnetoresistance graphene based spin valve and its application for realization of logic gates. *Physics Letters A*, *384*(7), p.126171.

[27] Hirohata, A., Yamada, K., Nakatani, Y., Prejbeanu, I.L., Dién y, B., Pirro, P. and Hillebrands, B., 2020. Review on spintronics: Principles and device applications. *Journal of Magnetism and Magnetic Materials*, *509*, p.166711.

[28] Parkin, S., Jiang, X., Kaiser, C., Panchula, A., Roche, K. and Samant, M., 2003. Magnetically engineered

spintronic sensors and memory. *Proceedings of the IEEE*, *91*(5), pp.661-680.

[29] Bowen, M., Cros, V., Petroff, F., Fert, A., Martınez Boubeta, C., Costa-Krämer, J.L., Anguita, J.V., Cebollada, A., Briones, F., De Teresa, J.M. and Morellón, L., 2001. Large magnetoresistance in Fe/MgO/FeCo (001) epitaxial tunnel junctions on GaAs (001). *Applied Physics Letters*, *79*(11), pp.1655-1657.

[30] Kubota, H., Fukushima, A., Yakushiji, K., Nagahama, T., Yuasa, S., Ando, K., Maehara, H., Nagamine, Y., Tsunekawa, K., Djayaprawira, D.D. and Watanabe, N., 2008. Quantitative measurement of voltage dependence of spin-transfer torque in MgO-based magnetic tunnel junctions. *Nature Physics*, *4*(1), pp.37-41.

[31] Moodera, J.S., Kinder, L.R., Wong, T.M. and Meservey, R., 1995. Large magnetoresistance at room temperature in ferromagnetic thin film tunnel junctions. *Physical review letters*, *74*(16), p.3273.

[32] Yuasa, S., Nagahama, T., Fukushima, A., Suzuki, Y. and Ando, K., 2004. Giant room-temperature magnetoresistance in single-crystal Fe/MgO/Fe magnetic tunnel junctions. *Nature materials*, *3*(12), pp.868-871.

[33] Wuttig, M., 2005. Towards a universal memory?. *Nature Materials*, *4*(4), pp.265-266.

[34] Liu, Q., Gao, S., Xu, L., Yue, W., Zhang, C., Kan, H., Li, Y. and Shen, G., 2022. Nanostructured perovskites for nonvolatile memory devices. *Chemical Society Reviews*, *51*(9), pp.3341-3379.

[35] Julliere, M., 1975. Tunneling between ferromagnetic films. *Physics Letters A*, *54*(3), pp.225-226.

[36] Sinha, R. and Kaur, J., 2022. Analyzing the impact of different composite dielectrics on performance parameters of a magnetic tunnel junction memory device. *Journal of Electronic Materials*, *51*(10), pp.5686-5703.

[37] Datta, D., Behin-Aein, B., Datta, S. and Salahuddin, S., 2011. Voltage asymmetry of spin-transfer torques. *IEEE Transactions on Nanotechnology*, *11*(2), pp.261-272.

[38] Sinha, R. and Kaur, J., 2022. Analyzing the impact of different composite dielectrics on performance parameters of a magnetic tunnel junction memory device. *Journal of Electronic Materials*, *51*(10), pp.5686-5703.

[39] Munira, K., Butler, W.H. and Ghosh, A.W., 2012. A quasi-analytical model for energy-delay-reliability tradeoff studies during write operations in a perpendicular STT-RAM cell. *IEEE transactions on electron devices*, *59*(8), pp.2221-2226.

[40] Uribe, M.D.R., Magana, A.J., Bahk, J.H. and Shakouri, A., 2016. Computational simulations as virtual laboratories for online engineering education: A case study in the field of thermoelectricity. *Computer Applications in Engineering Education*, *24*(3), pp. 428-442.